IMPROVED MECHANICAL SEAL DESIGN THROUGH MATHEMATICAL MODELLING

by

Richard F. Salant

Manager, Fluid Mechanics and Heat Transfer Department

and

William E. Key

Engineering Specialist

Roy C. Anderson Research Center

Borg-Warner Research Corporation

Des Plaines, Illinois

Richard F. Salant, Manager of the Fluid Mechanics and Heat Transfer Department at the Borg-Warner Research Center, received his B.S. (1963), M.S. (1963) and Sc.D. (1967) in Mechanical Engineering from M.I.T. Prior to joining Borg-Warner in 1972, he held faculty positions at M.I.T. (Associate Professor, Assistant Professor) and the University of California, Berkeley (Assistant Professor). His areas of research have included combustion, theoretical and experimental acoustics, fluid dynamics, heat transfer, and turbomachinery.

William E. Key, Engineering Specialist at the Borg-Warner Research Center, received his B.S. (1964) and M.S. (1967) from the University of California, Berkeley, and did postgraduate work in biophysics at the University of Western Ontario. Prior to joining Borg-Warner in 1974, he held positions at TRW Systems Group (member of the technical staff) and North American Rockwell (Research Engineer). His research has been in the areas of analytical and experimental fluid mechanics, with emphasis on numerical simulation.

ABSTRACT

The mechanical seal manufacturer can now offer the user new seal designs quickly and efficiently, and can respond to troubleshooting requests rapidly, through the use of modern, computerized, seal design techniques.

In particular, a mathematical model of a generalized mechanical seal has been constructed, which incorporates the fluid dynamics of the thin fluid film between the faces and the mechanical and thermal behavior of the various seal components. This model, in the form of a series of interactive computer programs, is used by the seal designer to predict the performance of a given seal design. The designer enters the seal geometry, physical properties of the seal and fluid, and the operating conditions as inputs. The computer programs then determine such seal characteristics as fluid film thickness, power dissipation, torque, leakage rate, deformation characteristics, and temperature distributions.

In developing a new seal, this mathematical model allows the designer to evaluate a large number of alternative designs without the necessity of extensive testing. In troubleshooting an existing seal, the model assists the designer in identifying the sources of problems, and correcting those problems through design changes.

This computerized seal model has been used to analyze a number of seals which have been built and tested. The model predictions agree well with test results.

INTRODUCTION

The design of mechanical seals has remained largely an art since the development of the first mechanical seals in the early 1900s. The seal designer relies primarily on past experience, physical intuition, some very basic calculations, and on a great deal of testing and empirical data. Until recently, he has had few analytical tools with which to work. This has made the development of new seals a time-consuming and expensive process. As the demands of more difficult services, tighter government restrictions, and more sophisticated customers become increasingly stringent, the need for more effective and efficient design methods increases.

Improved seal design methods must be based on physical understanding of the sealing process. However, over the last thirty-five years a great deal of research has been done on mechanical seals, yielding much fundamental understanding, but without having a substantial impact on seal design. This lack of impact stems from the complex geometries of seals. While seal research has been primarily directed towards simplified geometries (which help elucidate the physical phenomena of interest), the results of such research have not been successfully applied to actual commercial seals, because the complex geometries of the latter have not been readily amenable to analysis.

This situation is now changing. The rapid proliferation of computers over the last few years has led to the development of computer programs and hardware which are capable of handling complex seal geometries and which are accessible to the designer. Thus, it is believed it is now timely to apply the basic research results of the last thirty-five years to actual seals.

Such an effort is now underway, and has already achieved a degree of success. The objective of this work is the development of an analytical design tool for mechanical seals, to be used by the average designer, not the researcher. It would be utilized for the analysis of proposed seal designs and alternatives (before they are built), as well as for the troubleshooting of

existing seals. It should be emphasized that this tool is not intended to replace the designer, but rather to serve as a supplement to his other resources.

The approach followed in the present work is to apply existing theories of seal operation to an actual commercial seal, and compare the theoretical predictions with test results. On the basis of such a comparison, the most relevant theory (or theories) is selected and used to construct a mathematical model. The latter is put into a form suitable for use by a designer.

The model is not intended to be completely general and comprehensive, applicable to all types of seals under all conditions. Instead, it is comparatively simple, with many restrictions, but is expandable so that additional features may be added in the future. This model considers complex seal geometries (but they must be axisymmetric), single phase incompressible liquids, steady state operation, and spring-loaded seals (bellows seals are now included, but not discussed in this paper). The model does not consider vibration, misalignment, nor other dynamic effects.

THE SEALING INTERFACE

Conditions at the Interface

The most important portion of a mechanical seal is the interface between the two seal faces. It is here that the actual sealing takes place. Every other part of the seal is designed primarily to provide the proper conditions at this inerface for effective sealing. Hence, the overall design of a seal depends very strongly on the phenomena occuring at the interface.

There are three possible operating conditions at the interface. First, there could be a continuous fluid film over the entire interface, separating the two faces. Under such a condition, there must be a very small, but finite, gap between the faces. Second, there could be mechanical contact between the faces (asperity contact), corresponding to the boundary lubrication regime. Third, there could be a fluid film over part of the interface, and mechanical face contact over the other part.

For many years it was believed that sealing is achieved solely by mechanical contact between the faces. While this may have been the case for early, heavily loaded seals, it is not generally true for modern seals. During operation of the latter, as they experience transients in speed and load from start-up, shut down, and speed and pressure variation, it is likely that all three interface conditions are encountered at various times. Thus, the operation of a modern mechanical seal is quite complex. However, considerable simplification occurs if one considers only the steady state operation of such a seal.

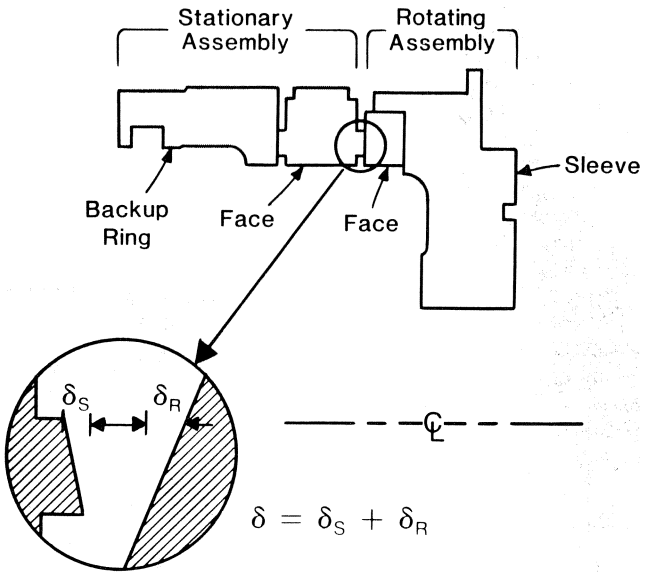

Figure 1. Schematic Drawing of Seal A.

Previous research studies have shown that lightly—to moderately—loaded seals (balance ratios between .5 and 1) in moderately viscous fluids (e.g., water, oil), under steady state conditions, operate with a continuous fluid film at the interface [1]. While this film is extremely thin, 50 to 200 microinches, it is finite. The existence of this film implies that there will always be some leakage. While the leakage may be so small as to be visually undetectable (it may evaporate), it is impossible to eliminate (unless special measures are taken).

To verify the existence of a continuous fluid film for the seals of interest in the present study, a particular "typical" seal has been selected for detailed study. This seal, designated Seal A, is shown in Figure 1. It is a commercially available seal, designed to operate in water at pressures up to 2000 psi and speeds up to 6000 rpm. It has a 6.5 inch balance diameter, a balance ratio of .75, and faces of carbon-graphite and tungsten carbide. Data generated by a series of tests on this seal (in a tester) have been analyzed in three different ways.

First, the torque variations with speed and load have been determined and compared with the known characteristics of continuous fluid films and boundary lubrication interfaces. Such a comparison has shown that Seal A operates with a fluid film. Second, the measured torque values have been used, in conjunction with a simple analytical model of a film, to compute a film thickness (assuming a film exists). This has yielded a film thickness of 87 microinches. Such a value is reasonable since it is larger than the roughness asperity height (10 microinches) and the waviness height (23 microinches) of the faces, but still small enough to limit leakage. Thus, this calculation supports the contention that a fluid film exists. Finally, the wear rate of the carbon-graphite face has been measured and compared with published values for continuous film and boundary lubrication regimes. This has further confirmed the existence of a fluid film. (Details of the above examination of Seal A can be found in [2].) Thus, on the basis of our own measurements, as well as previous investigations, it can be concluded that the seals of interest in the present study operate with a continuous fluid film, under steady state conditions.

Function of the Fluid Film and Design Strategy

It is not surprising that successful mechanical seals operate with a continuous fluid film, since such a film performs an important function: it prevents mechanical contact between the faces. This greatly reduces wear, energy dissipation, and the risk of mechanical and thermal damage. The primary task of the seal designer, then, is to design the seal so that:

a. a stable fluid film is maintained between the faces,

b. the film is thick enough to prevent mechanical contact,

c. the film is thin enough to prevent excessive leakage.

The film thickness is controlled by the position of the floating seal face. As shown in Figure 2, the latter is free to move in the axial direction. It will occupy an equilibrium position which is determined by the forces acting on it, as depicted schematically in Figure 2. Ignoring the spring force (which is insignificant in high pressure seals), it is seen that the net force tending to push the floating face toward the fixed face, the "closing force", is,

$$F_c = \Delta p A_f N_B, \qquad (1)$$

where the balance ration, $N_B = A'/A_f$. (2)

The "opening force", tending to push the floating face away from the fixed face, is produced by the pressure forces within the film and is given by,

$$F_o = \int_{A_f} p dA. \quad (3)$$

F_o will, in general, be a function of the separation between the two faces (the film thickness), because the pressure distribution within the film will depend on film thickness. Thus, the floating face will assume a position (and the film thickness will be fixed) such that,

$$F_o = F_c, \quad (4)$$

and the floating face will be in equilibrium. Therefore, to determine the film thickness it is necessary to understand the pressure distribution within the film.

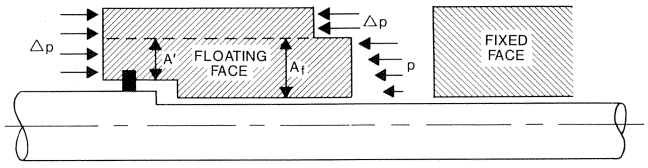

Figure 2. Forces on the Floating Seal Face.

Pressures within the Film

Before the pressure distribution within the film can be computed, it is necessary to adopt a model of the flow field. The simplest such model postulates that the seal faces are perfectly flat, smooth and parallel, producing a uniform fluid film (constant film thickness) with flow through the seal gap from the high pressure side to the low pressure side. For this model, the fluid mechanics equations can be solved in closed form to give an expression for the pressure distribution [3]. In the case in which the seal width is much smaller than the average radius (applicable to most seals), this expression reduces to a linear pressure distribution, i.e., the pressure drops linearly with radial position from the high pressure side to the low pressure. The opening force, as expressed by Equation (3), then becomes,

$$F_o = .5\Delta p A_f, \quad (5)$$

and the force balance, Equation (4), becomes,

$$\Delta p A_f N_B = .5\Delta p A_f. \quad (6)$$

Equation (6) indicates that this simple seal model is unrealistic for two reasons. First, since the opening force is independent of film thickness, Equation (5), this model does not yield a unique film thickness; i.e., the seal should operate with any film thickness. This is incorrect. Second, Equation (6) states that only seals with a balance ratio of .5 can operate with a film. This, too, is incorrect, since seals with balance ratios as high as .85 (or even higher) perform well.

It is clear that the simple seal model, described above, predicts too low an opening force ($.5\Delta p A_f$) to correspond to reality. Thus, there must be some other physical mechanism which produces higher pressures within the film, and, therefore, a higher opening force. Much of the seal research done over the last thirty-five years has dealt with such so-called load support mechanisms. The most important of these are based on effects produced by face roughness, face waviness, misalignment, and/or eccentricity, and face deformation. Each of these features has been shown to increase the pressures within the film. The first three are termed "hydrodynamic mechanisms" because they rely on the rotation of one of the faces to be operable. The last is termed a "hydrostatic mechanism," because it is operable even in the absence of rotation. In the present study, rather than including all of these mechanisms in the mathematical model, it has been decided to first determine the significance of each for the class of seals of interest.

The opening force, F_o, for Seal A has been determined from experimental measurements over a range of operating conditions. The contributions to F_o of each of the four load support mechanisms, discussed above, have been computed from the relevant theoretically derived equations. These calculations have shown that roughness, waviness, and misalignment/eccentricity produce insignificant contributions to the opening force. Only the deformation mechanism is important [2].

It has, therefore, been concluded that for the class of seals of interest, face deformation is the controlling mechanism for load support. Hence, the mathematical model needs only consider the deformation mechanism.

The Deformation Mechanism

Face Deformation

The deformation mechanism is based on the premise that the seal faces are not perfectly flat and parallel with a fluid film of constant thickness, but rather deform to be nonparallel with a variable film thickness. It is this nonuniform film thickness which can give rise to increased pressures within the film, and therefore increased load support.

Figure 1 contains a schematic diagram of Seal A, with a blown-up view of the interface region in which the deformations have been exaggerated. It is assumed that the seal deforms axisymmetrically, so that the faces converge or diverge in the radial direction, going from OD to ID (Figure 1 shows them converging). The amount of deformation of the stationary face is measured by δ_S, and that of the rotating face by δ_R, as shown in the figure. (Note that for Seal A, the stationary face floats in the axial direction and the rotating face floats in the axial direction and the rotating face is fixed). The total deformation is defined as,

$$\delta \equiv \delta_S + \delta_R. \quad (7)$$

A positive value of δ indicates a converging gap (from OD to ID), while a negative value indicates a diverging gap. For convenience, it is assumed that the high pressure side of the seal is at the OD, although this is not necessary to the model.

Since there is a continuous fluid film between the faces, there will be fluid flow from OD to ID, i.e., leakage. Since steady state is assumed, this flow is steady and the flow rate very low since the film thickness is very small. The variation of the film thickness with radius is taken to be of the form,

$$h = Ar^B, \quad (8)$$

where the constants A and B are related to the deformation and other seal parameters by,

$$A \equiv h_i/R_i^B, \quad (9)$$

$$B \equiv \frac{\ell n(1 + \delta/h_i)}{\ell n \alpha}, \quad (10)$$

$$\delta \equiv h_o - h_i \quad (11)$$

B is a measure of the convergence or divergence of the film. A positive B indicates convergence, a negative B divergence, and zero B a uniform film.

Fluid Mechanics Analysis of the Film

The governing fluid mechanics equations for the flow in the converging or diverging fluid film can be solved to yield a closed form expression for the pressure distribution (see Appendix). This distribution is shown in Figure 3. It is seen that converging films produce convex pressure profiles, while diverging films produce concave profiles. The greater the amount of convergence/divergence, the greater the degree of convexity/concavity. Since the opening force is equal to the integral of the pressure over the face, it is clear that converging films produce larger opening forces than a uniform film. In fact, forces large enough to hold in equilibrium seals with balance ratios between .5 and 1 can be generated, depending on the amount of convergence. Conversely, diverging films produce lower opening forces than a uniform film, and correspond to balance ratios between 0 and .5.

A converging film will tend to be stable while a diverging film will tend to be unstable, as is indicated in Figure 3. First, consider a converging film. If there is a sudden increase in film thickness due to an external disturbance (without a change in δ), the amount of convergence (δ/h_i or B) will decrease, and therefore the opening force will decrease. The imbalance between the closing and opening forces will then return the floating face to its original position. Similarly, a sudden decrease in film thickness will result in an increase in opening force, again returning the floating face to its original position. Conversely, for a diverging film, perturbations in the position of the floating face produce force changes which move the floating face away from its equilibrium position, an unstable condition.

Thus, it is clear that a satisfactory seal requires a design which produces a converging film. The remainder of this paper considers only this case.

For a seal with a given geometry, the larger the value of δ/h_i (and therefore B), the greater the degree of convexity of the pressure profile, and the greater the opening force, as is seen in Figure 3. Therefore, for a given seal with a given deformation δ, the floating face will assume an equilibrium position corresponding to a particular value of h_i. The latter will be that value

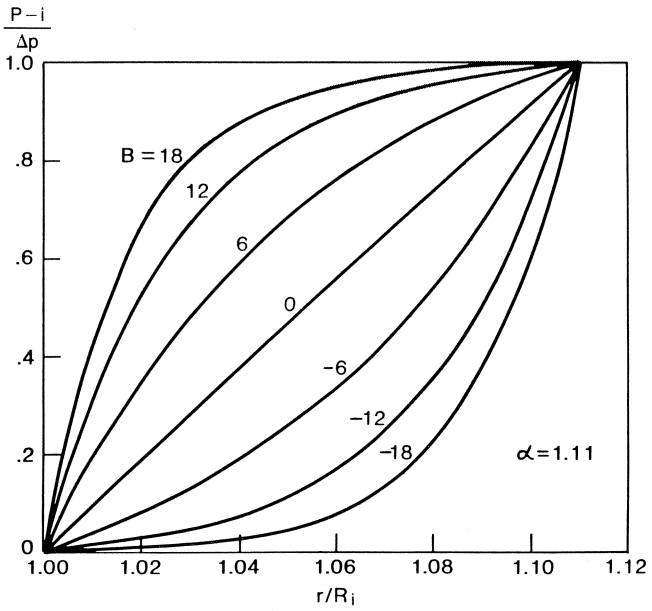

Figure 3. Pressure Distribution in Fluid Film.

which produces a value of δ/h_i (and hence B) corresponding to the particular pressure profile in Figure 3, which yields an opening force exactly equal to the closing force given by Equation (1). Thus, for a given seal, there is a unique film thickness h_i for each operating condition.

For any given seal geometry (N_B and α), one can calculate the closing force (from Equation (1)) and the pressure profile in the film for various values of δ/h_i. Therefore, one can compute the value of δ/h_i necessary for equilibrium. This procedure is contained in the Appendix. It is seen, therefore, that δ/h_i is a function only of the seal geometry, i.e.,

$$\delta/h_i = C_1 (\alpha, N_B) \tag{12}$$

Thus, for a given seal δ/h_i is a constant. This implies that the film thickness is directly proportional to the deformation; i.e., the larger the deformation, the larger the film thickness.

It is therefore seen that to control film thickness, the designer must control the deformation of the seal faces. First, he must design the seal to have positive deformation (converging film). Second, he must design in enough deformation to produce a thick enough film to avoid face contact (h_i must be significantly larger than the asperity height). Note that this contradicts a traditional view held by many seal designers that the ideal seal contains no deformation. Third, the designer must make sure that the deformation is small enough to avoid excessive leakage.

As stated above, one can calculate the equilibrium value of δ/h_i for a particular seal design. Therefore, if one knew the deformation δ, one could easily compute the film thickness. Once the film thickness and deformation are known, all other important characteristics of the seal can be calculated. Equations for the leakage rate, torque and energy dissipation rate, obtained from the solution of the governing fluid mechanics equations, are given in the Appendix. After the energy dissipation rate is obtained, the appropriate heat transfer equations can be solved to yield temperature distributions in the various seal components.

Thus, it is seen that the key to determining the behavior of the seal is the calculation of the seal deformation. This deformation consists of two parts: mechanical deformation and thermal deformation. While the mechanical deformation depends on the pressure loading on the seal (and any other applied forces), the thermal deformation depends on the heat transfer into the seal which, in turn, depends on the energy dissipation rate. Since the latter depends on the film thickness (see Equation (A7) in Appendix), it is not possible to solve for δ, h_i, and all other quantities sequentially. Rather, the deformation and film thickness must be solved for simultaneously.

Deformation Analysis

To determine the deformation δ, not only must the seal faces be considered, but the entire supporting structure must be considered. However, regardless of the structural details, if linear materials are considered, the deformation can be expressed by the following general equation,

$$\delta_{S,R} = K_n K_p \Delta p + K_g K_f H + K_r F_s \tag{13}$$

The constants in the above equation, K's, are termed "influence coefficients." They have fixed values for any particular seal design, and those values are dependent on the structural details. The first term in Equation (13) represents the mechanical deformation, and the second term the thermal deformation. The third term represents the deformation of a face caused by the shear force exerted on that face by its backup ring or holder. However, if the face is always in sliding contact with its backup

ring, as is assumed in the present study, the third term can be absorbed into the first term (since F_s can be expressed in terms of Δp).

Equation (13) could be used to calculate the deformations as functions of Δp and H if one knew the values of the influence coefficients for the particular seal of interest. To obtain the influence coefficients, numerical structural analyses are performed on the entire seal to yield δ_S and δ_R for four particular hypothetical operating conditions. From these calculated values of δ_S and δ_R one can compute the values of the Ks (for the procedure, see [4]). This allows one, then, to compute δ_S and δ_R for any operating condition without further structural analysis.

In the present model, the structural analyses (at the four hypothetical operating conditions) are performed with the commercially available computer program ANSYS.

Each seal face, its holder, and all other components with which it is in contact, are treated together as an assembly. Any number of components in an assembly can be handled. Similarly, any number of assemblies, either rotating or stationary, can be analyzed. This allows analysis of multiple seal systems, such as double and tandem seals. For each mating pair of assemblies, a force balance on the floating face is used to determine the opening force. That, together with the known form of the pressure distribution in the film, yields the latter distribution. The pressure distribution is then inserted into a force balance on the fixed assembly, which yields the restraining force on that assembly. Once all the forces around each assembly are determined, ANSYS is used to perform a finite element analysis of each assembly. It calculates the stresses, strains, and mechanical deformations at each internal grid point (specified by a mesh generating program) within the assembly.

Analysis of thermal deformation requires computation of the temperature distribution in all seal components. The energy dissipated in the film is accounted for by treating the film as a heat source, with strength arbitrarily set at one horsepower (temperature profiles for any heat source strength can be scaled-up). The heat transfer from the film into the faces is apportioned between the faces in inverse proportion to their thermal resistances. Specification of the heat transfer coefficients along the entire periphery of all seal components is done by treating each surface as a rotating or stationary, cylindrical or disc-like surface, and using laboratory-generated coefficients for such surfaces.

Utilizing the above information, ANSYS performs thermal analyses, thermal deformation analyses, and mechanical deformation analyses. Hence, all the influence coefficients can be determined.

Computation of Seal Characteristics

As mentioned previously, for the present model the deformation equation, Equation (13), can be simplified to the form,

$$\delta = C_2\Delta p + C_3 H \qquad (14)$$

where C_2 and C_3 are determined from the influence coefficients of the individual faces.

The energy dissipation rate H, as described earlier, is dependent on the film thickness h_{av}, and is given by Equation (A7). By combining Equation (14) with Equations (12) and (A7), one obtains a single algebraic equation for the energy dissipation rate,

$$H = \frac{-C_2\Delta p}{2C_3} + \left[\left(\frac{C_2\Delta p}{2C_3}\right)^2 + \frac{C_1\mu A_f U^2}{C_r C_3(1+.5C_1)}\right]^{1/2} \qquad (15)$$

Thus, once the influence coefficients are calculated, H can be computed. Then δ can be calculated from Equation (14), h_i from Equation (12), and Q from Equation (A5).

FORM OF MATHEMATICAL SEAL MODEL

The mathematical seal model, described in the previous sections, has been put in the form of a series of interactive computer programs. These programs are intended to be used by designers, who do not necessarily have detailed knowledge of the contents of the programs. They, therefore, contain many prompts which ask the designer for information and give him instructions, leading him through the sequence. The programs also contain many safeguards and error statements to avoid incorrect and aborted runs. The sequence of operations has been arranged so that modifications and variations of a design can be analyzed without rerunning all computations. An average basic seal analysis takes one to three days (actual time, not computer time), depending on complexity of the design. Once a basic analysis has been performed, analysis of modifications usually requires a few hours (or less). The lagest portions of these times are spent on specification of the problem, interpretation of drawings, and conversion of drawings to data files.

The sequence of operations starts with the designer inputting the seal geometry, which is used to generate finite element meshes for all seal components. Then, the forces and heat loads on the various components are computed. Utilizing this information, ANSYS performs finite element thermal and deformation analyses for the four hypothetical operating conditions required for determination of the influence coefficients. The influence coefficients are then computed, and finally the seal characteristics (e.g., film thickness, leakage rate, etc.) are calculated for various operating conditions. If desired, the programs can be run without the use of influence coefficients, in which case the thermal and deformation analyses are performed at the operating conditions of interest.

When the analysis is completed, the designer is provided with the seal performance characteristics; a typical printout is shown in Figure 4. For each speed, a table is generated giving h_1, δ, h_{av}, T, H, f, Q and face temperature as functions of pressure. The deformation equations for all seal faces are also provided. In addition, as the programs are being run, the designer can call for intermediate information, which is often very useful in evaluating the details of a seal design and in

Example Seal:
-FILM THICKNESS vs PRESSURE & RPM-

LEFT FACE: DELTA = -0.1216*DP + 43.2*H
RIGHT FACE: DELTA = -0.0246*DP + 54.7*H
TOTAL: DELTA = -0.1462*DP + 97.4*H

FLUID TEMP = 120 (WATER)
BALANCE = 0.650

SHAFT SPEED = 3500 RPM

PRESSURE psi	PRESSURE bar	h1 muinch	delta muinch	have muinch	TQ lb*ft	H hp	f	QLEAK cc/min	TFACE deg F
100	6.9	102.7	76.6	141.0	1.40	0.94	0.0112	12.76	142
200	13.8	96.3	71.8	132.2	1.56	1.04	0.0062	20.24	145
300	20.7	90.1	67.2	123.7	1.71	1.14	0.0045	24.20	147
400	27.6	84.5	63.0	116.0	1.87	1.25	0.0037	25.94	150
500	34.5	79.4	59.2	109.0	2.04	1.36	0.0032	26.28	152
600	41.4	74.7	55.7	102.6	2.21	1.47	0.0029	25.76	155
700	48.3	70.4	52.5	96.7	2.39	1.59	0.0027	24.74	158
800	55.2	65.9	49.2	90.5	2.56	1.71	0.0025	23.10	161

SHAFT SPEED = 4500 RPM

PRESSURE psi	PRESSURE bar	h1 muinch	delta muinch	have muinch	TQ lb*ft	H hp	f	QLEAK cc/min	TFACE deg F
100	6.9	123.1	91.8	169.0	1.28	1.09	0.0101	25.97	146
200	13.8	116.6	86.9	160.0	1.39	1.19	0.0055	42.67	148
300	20.7	110.2	82.2	151.3	1.51	1.29	0.0040	52.72	151
400	27.6	103.7	77.3	142.4	1.63	1.39	0.0032	57.76	153
500	34.5	98.1	73.2	134.7	1.75	1.50	0.0028	60.02	156
600	41.4	93.0	69.4	127.7	1.88	1.61	0.0025	60.25	158
700	48.3	88.3	65.8	121.2	2.02	1.73	0.0023	59.16	161
800	55.2	83.9	62.6	115.2	2.15	1.84	0.0021	57.24	164

Figure 4. Typical Computer Printout.

deciding on modifications. For example, he can ask for drawings of the deformed components, plots of isotherms, the values of the temperature and displacement at any point, and the coefficients of intermediate equations (e.g. influence coefficients).

EXAMPLES OF MODEL USE

The value of any mathematical model is ultimately dependent on how well it corresponds to reality. The seal model, described in the previous sections, has been used to analyze and troubleshoot many different seal designs. Generally, the results agree well with observed seal behavior. Four examples follow.

Seal A

Seal A, shown in Figure 1, has been described earlier. It is a commercial seal, and many years of experience have shown it to be very well-behaved, exhibiting little leakage and good stability. A unique feature of this seal is its ability to perform just as well at the upper end of its pressure range (2000 psi) as at the lower end.

The mathematical seal model has been used to compute the performance characteristics of this seal over a range of pressure and speed. Figure 5 shows computed curves of the friction coefficient f versus the duty parameter G (a measure of speed and load). Also shown in Figure 5 are experimental points, which have been obtained by running this seal in a tester. It is seen that the agreement between the model predictions and the experimental results are quite good.

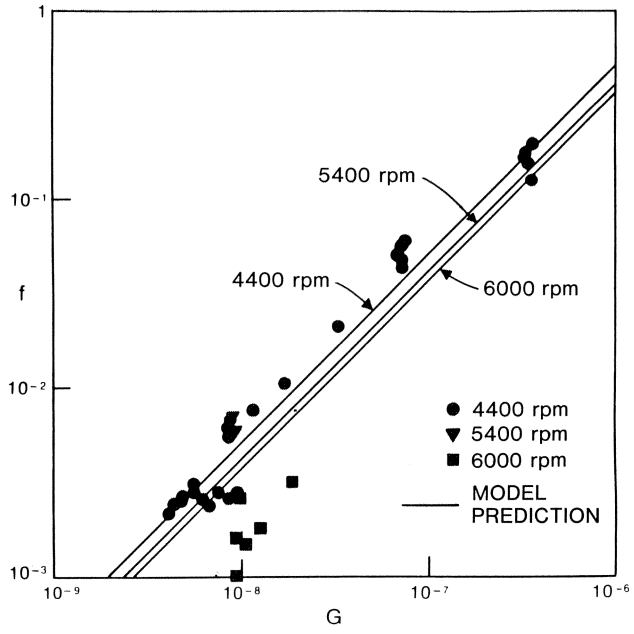

Figure 5. f vs. G, Seal A.

The predicted film thickness is plotted as a function of speed in Figure 6. For the practical operating range (1800-6000 rpm), the model predicts an average film thickness of 45 to 140 microinches. In comparison to the roughness and waviness heights of the faces, these thicknesses are large enough to prevent face contact, but still small enough to prevent excessive leakage. Thus, these results agree with the experienced good behavior of this seal.

The mathematical seal model also predicts the film thickness to be substantially independent of pressure (as implied in Figure 6). This agrees with the experimental observation that the seal performs in a similar manner over its entire pressure range. The reason for this insensitivity to pressure can be seen from the deformation equations generated by the model,

$$\begin{aligned} \delta_S &= -.0664\Delta p + 14.38H \\ \delta_R &= .0716\Delta p + 28.55H \\ \delta &= .0052\Delta p + 42.93H \end{aligned} \quad (16)$$

(In the above equations, δ is in microinches, Δp in psi, H in horsepower).

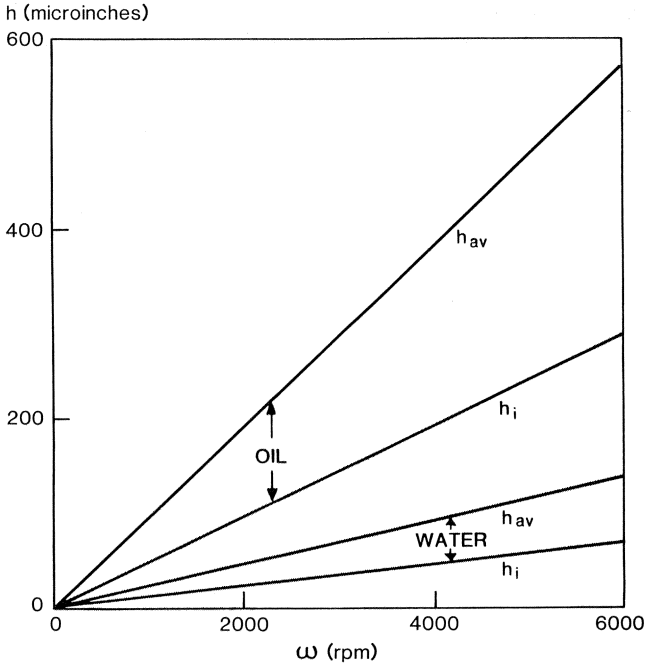

Figure 6. h vs. ω, Seal A.

These equations show that while both seal faces undergo mechanical deformation, which is pressure dependent, such deformation is negative for the stationary face, positive for the rotating face, and both are of nearly the same magnitude. Thus, the two mechanical deformations cancel each other, and do not affect the film. This can be further seen from Figures 7 and 8, which show the deformed shapes of the faces predicted by the model, under pressure loading alone (no thermal loading). Note that the broken lines on the figures represent the undeformed shapes, and the deformations are exaggerated for clarity.

Seal A performs well with water, for which it has been designed. However, if used with oil it leaks excessively, which agrees with the model predictions. Film thicknesses with oil are substantially larger than those with water, as shown in Figure 6. This is because the energy dissipation rate with oil is higher (due to the higher viscosity), leading to larger thermal deformations, and therefore a thicker film. Since the leakage rate varies with the cube of the film thickness, and only inversely with viscosity, it will be much larger with oil.

Seals B and C

In contrast to Seal A, Seals B and C are known to have design effects. They are preliminary designs for the primary and closure seals in a seal system for pumps in an LNG pipeline. They are shown in Figure 9, have balance diameters of 6.5 inches, balance ratios of .82, and tungsten carbide and carbon-graphite faces. Their operating point is 800 psi and 5000 rpm.

Test seals built according to these designs have performed unsatisfactorily, experiencing severe wear. Hence, it was necessary to redesign these seals to achieve satisfactory operation. However, the preliminary designs (Figure 9) serve as a good test case for the mathematical model.

Model predictions of film thickness as a function of speed are shown in Figure 10. In contrast to Seal A, the film thicknesses are pressure dependent, decreasing with increasing pressure. At the operating point, the film thicknesses are 2.4 microinches and .5 microinches. Since these are significantly smaller than the asperity height of 10 microinches, it is clear there will be mechanical contact between the faces, and continuous films cannot be maintained. This is in agreement with the known behavior of these seals.

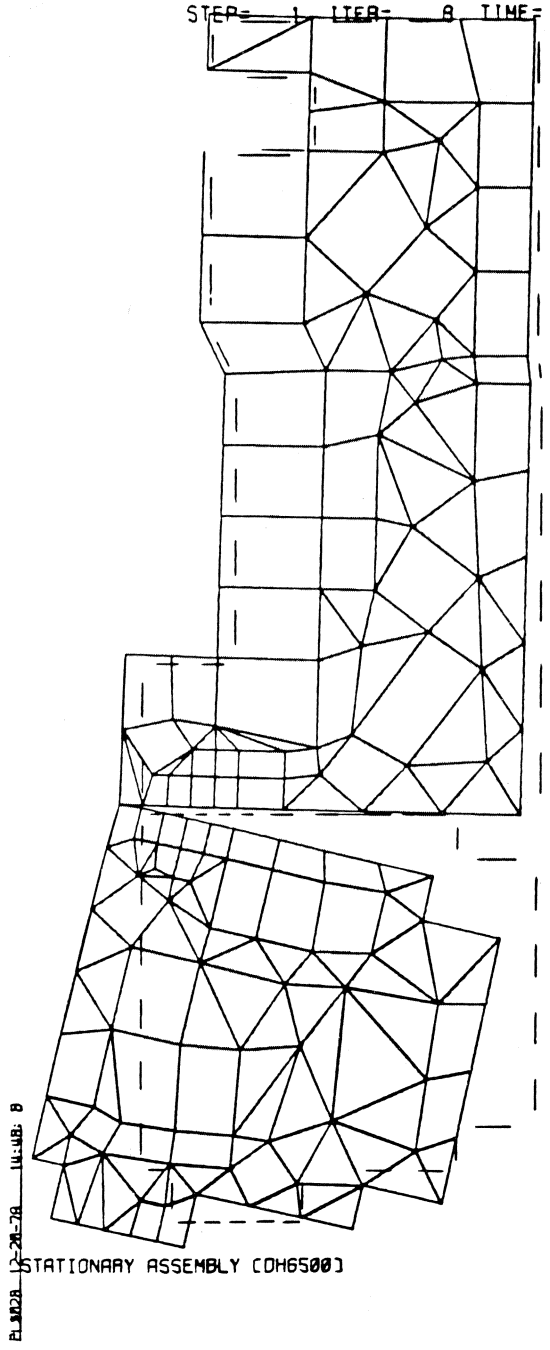

Figure 7. Deformation of Stationary Assembly, Seal A.

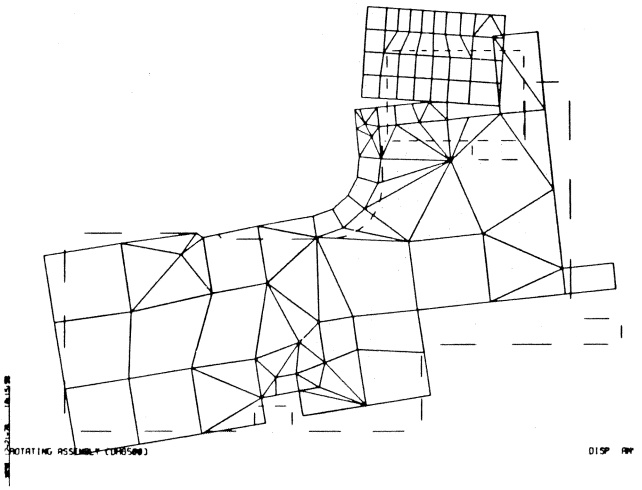

Figure 8. Deformation of Rotating Assembly, Seal A.

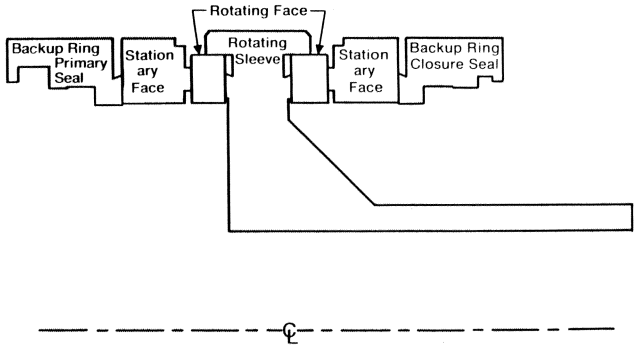

Figure 9. Schematic Drawing of Seals B and C.

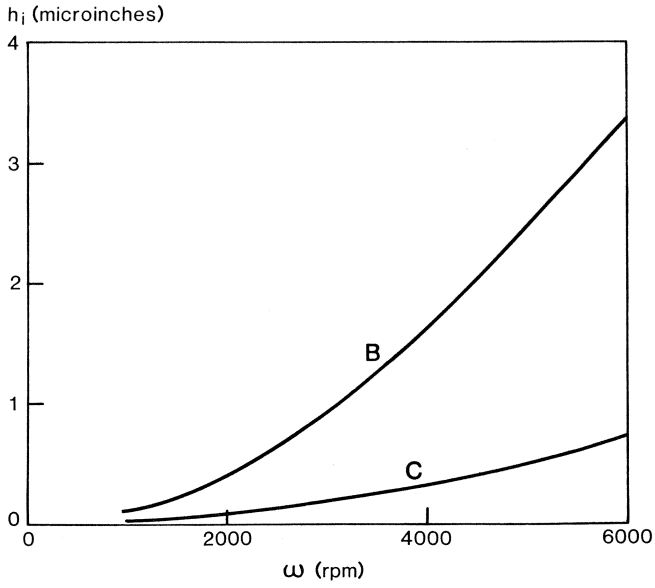

Figure 10. h_i vs. ω, Seals B and C.

The predicted deformation equations reveal the reason for the breakdown of the films.

Seal B

$$\delta = -.1280\Delta p + 10.2771H \quad (17)$$

Seal C

$$\delta = -.1276\Delta p + 1.8404H \quad (18)$$

Comparing Equations (17) and (18) with the equivalent expression for Seal A, Equation (16) indicates that Seals B and C experience too much negative mechanical deformation and not enough positive thermal deformation to maintain a film.

Seal D

Seal D illustrates how very subtle changes in geometry can produce large changes in seal performance. This seal, shown in Figure 11, has been designed for use in boiler feedwater pumps. It has a 6.5 inch balance diameter, .65 balance ratio, and tungsten carbide and carbon-graphite faces. Its operating point is 580 psi and 4500 rpm.

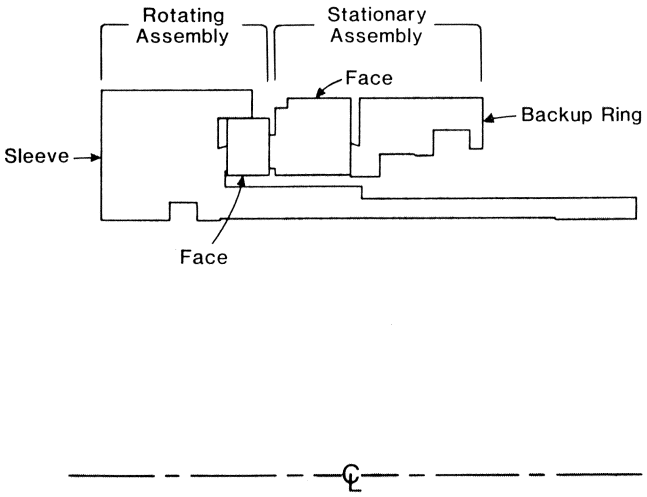

Figure 11. Schematic Drawing of Seals B and C.

In actual use, this seal has experienced a number of structural failures of the tungsten face. To determine if this is due to a design flaw, a complete analysis has been performed. The predicted film thicknesses, shown in Figure 12, indicate that the seal should operate at its design point with a continuous fluid film. No design defect has been found. Subsequently, it was determined that the seal failures were related to water quality and the formation of mineral deposits. When water quality was improved, the seal performed well, confirming the model predictions.

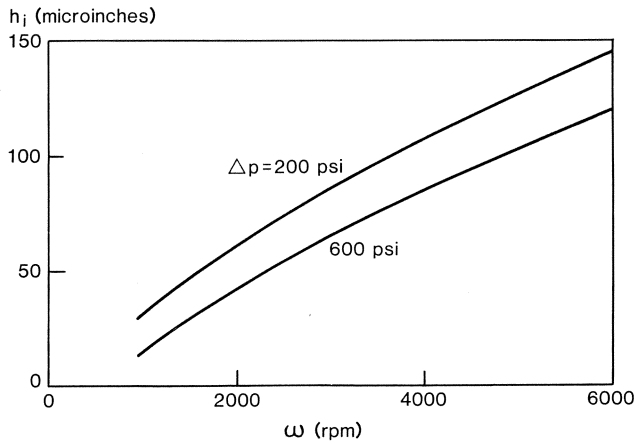

Figure 12. h_i vs. ω, Seal D.

However, tests have also shown that this seal requires a very high starting torque. In a tester, the motor cannot be started while the system is fully pressurized. The reason for this can be seen from the predicted deformation equations.

$$\delta = -.1362\Delta p + 43.4H$$
$$\delta = -.0284\Delta p + 51.6H$$
$$\delta = -.1646\Delta p + 95.0H \quad (19)$$

Equation (19), together with Figure 12, indicates that although there is significant negative mechanical deformation, under steady conditions there is sufficient positive thermal deformation to overcome the mechanical deformation and produce a film. However, at start-up there is virtually no thermal deformation and the seal gap is diverging, resulting in mechanical contact and high torque.

To reduce the starting torque, the seal design has been modified to produce positive mechanical deformation, as shown in Figure 13. A small cutout has been made in the stationary face, and two shoulders in the rotating face holder have been moved. The large effect produced by the latter change can be seen in Figures 14 and 15 which contain deformation shapes generated by the mathematical model. The deformation equations for the modified design are,

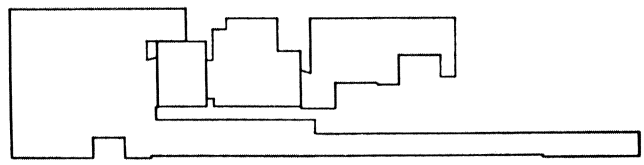

Figure 13. Schematic Drawing of Modified Seal D.

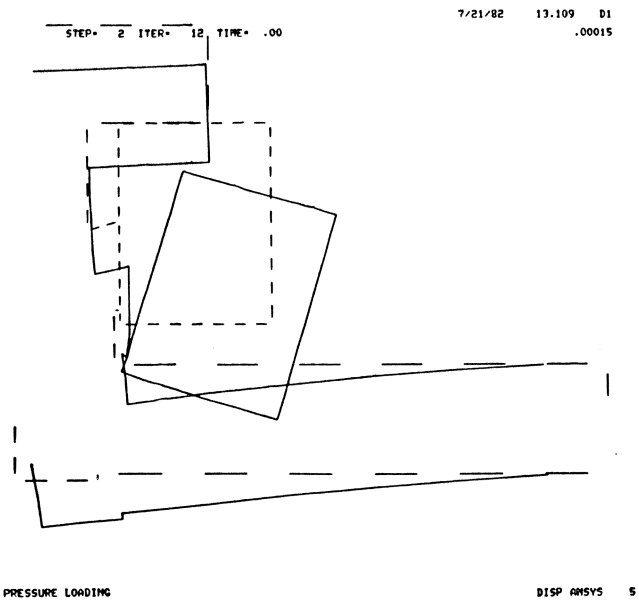

Figure 14. Deformation of Rotating Face, Seal D.

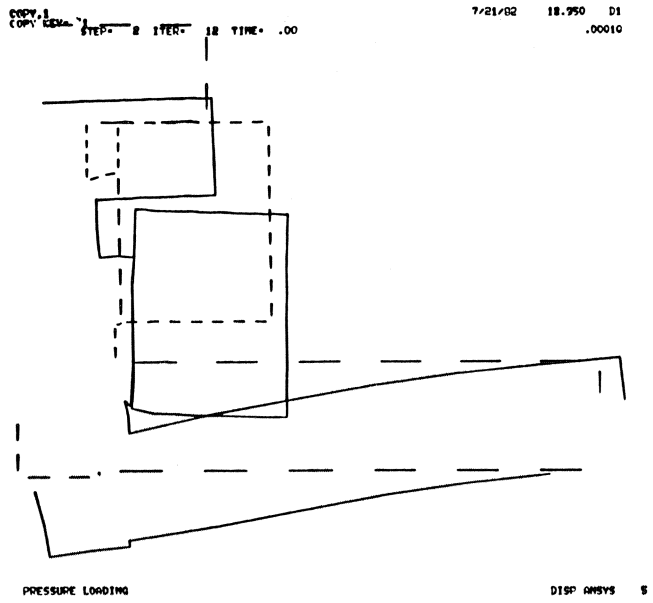

Figure 15. Deformation of Rotating Face, Modified Seal D.

$$\delta_S = .0295\Delta p + 47.1H$$
$$\delta_R = .0061\Delta p + 47.5H$$
$$\delta = .0356\Delta p + 94.6H \qquad (20)$$

Thus, it is clear that the goal of positive mechanical deformation has been achieved. This has been confirmed by tests on the modified design; in fact, the starting torque is so low that the shaft of the tester can be turned by hand with the system fully pressurized.

CONCLUSIONS

From the results reported above, it can be concluded that mathematical modelling provides the designer with a quantitative analytical tool which can be used to predict the performance of prospective seal designs. It is easy to use and yields results quickly. Such quantities as film thickness, face deformation, torque, leakage, and face temperature can be estimated before a seal is built. Experimental results for a number of seals have agreed well with model predictions. While the model developed thus far is not completely general, it has proved extremely useful, and is now routinely utilized for seal evaluation, and as a guide for planning seal test programs.

NOMENCLATURE

A	Constant defined by Equation (8)
A_f	face area
A′	area defined by Figure 2
B	constant defined by Equation (10)
C_1	function of α and N_B defined by Equations (A2)-(A4)
C_2, C_3	coefficients defined by Equation (14)
C_r	correction factor to account for surface roughness, computed using equation from [5]
f	friction factor
F_c	closing force on floating seal face
F_o	opening force on floating seal face
G	duty parameter, $\mu U(R_o\text{-}R_i)/F_c$
h	film thickness
h_{av}	average film thickness
h_i	film thickness at ID
h_o	film thickness at OD
H	energy dissipation rate
K_f, K_g, K_n, K_p, K_r	influence coefficients
N_B	balance ratio
N_w	function defined by Equation (A3)
p	pressure
p_i	pressure at ID
Q	leakage flow rate
r	radial coordinate
R_b	balance radius
R_i	inner radius
R_o	outer radius
T	torque
U	average face speed
α	ratio of outer radius to inner radius
Δp	pressure drop across seal
δ	deformation of seal
δ_R	deformation of rotating face
δ_S	deformation of stationary face
ω	angular speed

APPENDIX

Reynolds equation can be solved for flow in the converging or diverging film of Equation (8), to yield the pressure distribution,

$$\frac{p - p_i}{\Delta p} = \frac{1 - (R_i/r)^{3B}}{1 - \alpha^{-3B}} \qquad \text{For } B \neq 0$$
$$= \frac{\ell n\,(R_i/r)}{\ell n\,(1/\alpha)} \qquad \text{For } B = 0 \qquad (A1)$$

Inserting Equation (A1) into Equation (3) and using Equations (4) and (1) results in,

$$N_w = 1/2\,(\alpha^2 - 1)N_B \qquad (A2)$$

where,

$$N_w \equiv \frac{(\alpha^2 - 1)/2 - (\alpha^{2-3B} - 1)/(2 - 3B)}{(1 - \alpha^{-3B})} \qquad \text{For } B \neq 0$$
$$\equiv \frac{(\alpha^2/2)\,\ell n\,\alpha - (\alpha^2 - 1)/4}{\ell n\,\alpha} \qquad \text{For } B = 0 \qquad (A3)$$

From Equation (8) it is seen,

$$\delta/h_i = C_1\,(\alpha, N_B) \qquad (A4)$$

From the solution of Reynolds equation,

$$Q = \left(\frac{\Delta p}{1 - \alpha^{-3B}}\right) \frac{C_r \pi B h_i^3}{2\mu} \qquad (A5)$$

between 2 and 5. Pumps with large nozzles relative to impeller diameter (case size) require thicker feet. Reinforcement of the volute wall in the vicinity of the pump feet has been provided so that the local case thickness is never less than one-third of the foot thickness.

The change made in the hold-down capscrews to achieve the 0.0015 inch shaft displacement criteria is also illustrated in Figure 2. Capscrews generally increase by about 4 sizes, i.e., from ¾ inch-10 to 1¼ inch-7. To accommodate the larger capscrews, the pump foot pads are frequently increased in length and/or width. For duplicate 5th Edition pumps, this added material is milled away and the original smaller diameter capscrew holes are drilled. Longer capscrews must be furnished due to increased foot thickness.

Pictures of a 6th Edition baseplate are featured in Figures 3 and 4. These pictures illustrate the revised method of attaching the support pedestals to the baseplate. As can be seen, the support pedestals are welded directly to a 1 inch to 1-½ inch thick deckplate that is in turn attached to the baseplate structural members by continuous fillet welds ⅜ inch to ½ inch in size. The heavy deckplate with no pedestal "cut-outs" significantly reduces any local plate deformation and permits the use of large support pedestal attachment welds (⅜ inch to ¾ inch). The degree of "fixity" at the support pedestal to baseplate interface increases with weld size. Support pedestals on 5th Edition process pump baseplates (Figure 5) were attached to the structural members (short sides only) and to the quarter inch thick deckplate. The attachment weld size (⅛ inch-⅜ inch) was limited by the thickness of the structural members and the deckplate.

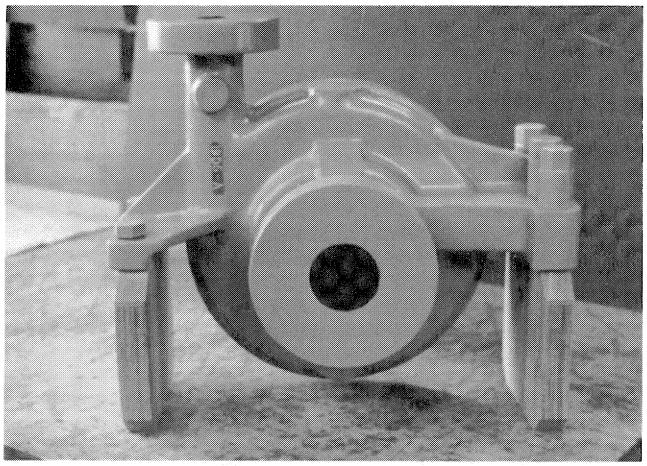

Figure 2. Modified Fifth/Sixth Edition Overhung Process Pump Case Pattern (1½ × 11 TC).

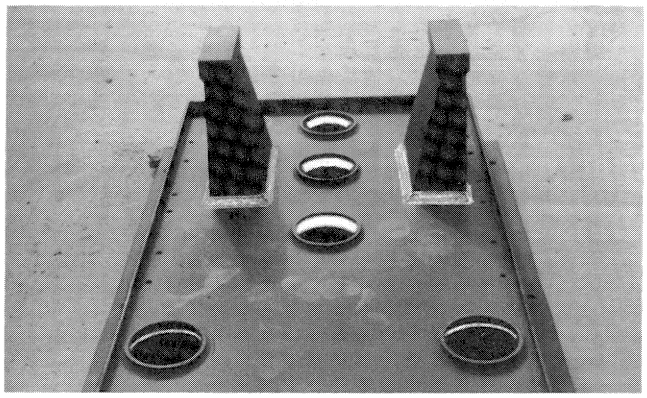

Figure 3. Topside View of a Sixth Edition Angle Type Baseplate.

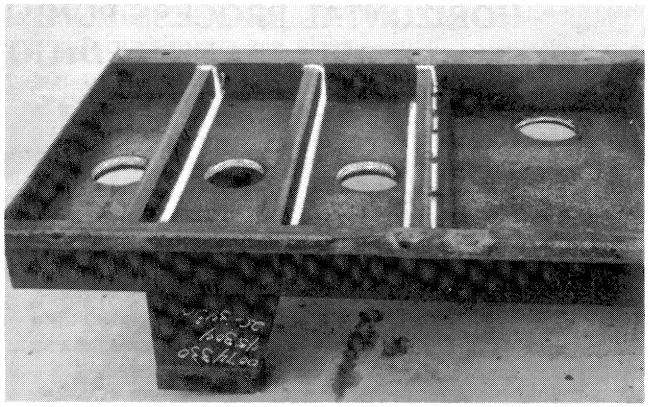

Figure 4. Underside View of a Sixth Edition Angle Type Baseplate.

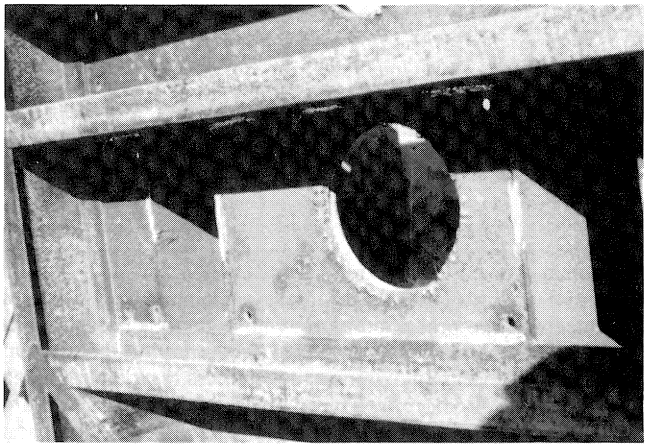

Figure 5. Underside View of a Fifth Edition Angle Type Baseplate.

ANALYTICAL WORK

The design modifications previously described are the consequence of our stiffness criteria and the associated analytical sizing procedures. Changes to either the stiffness criteria or the sizing procedures could result in different equipment modifications. For this reason, it is important to understand the equations and inherent assumptions made in the sizing procedures.

The sizing equations shown on the following pages have been derived for AP-610 Table 2 Nozzle Loads (Figure 6). These component loads are unsigned and, therefore, define direction and magnitude range. This means that each nozzle can be subjected to an infinite number of loading conditions. This obstacle has been overcome by defining a worst case condition for each of the three major subcomponents. The following text describes the equations and assumptions inherent in each subcomponent sizing procedure.

The Pump Casing

Previous research has demonstrated that overhung process pumps are most sensitive to moments about the Z axis [2]. This is attributable to a lack of torsional rigidity in the pump feet which transmit piping loads from the relatively stiff pump casing to the support pedestals. By comparing pump case geometry, the same statement can be made of one and two stage double bearing process pumps. Knowing this fact and by making the following simplifying assumptions, one can develop three equa-

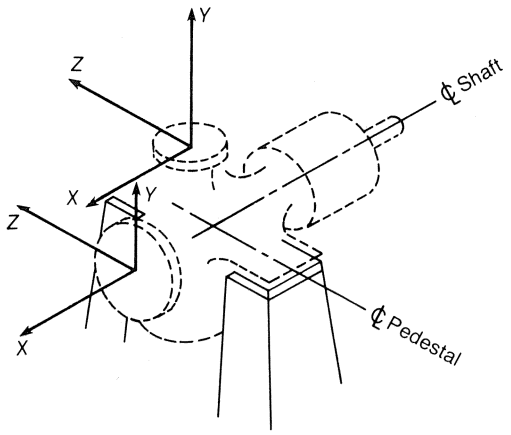

—Coordinate System for the Forces and Moments in Table 2

Table 2—Nozzle Loadings

Force/Moment[a]	Nominal Size of Nozzle Flange (inches)								
	≤2	3	4	6	8	10	12	14[b]	16[b]
Each top nozzle									
F_x	160	240	320	560	850	1200	1500	1600	1900
F_y (compression)	200	300	400	700	1100	1500	1800	2000	2300
F_y (tension)	100	150	200	350	530	750	920	1000	1200
F_z	130	200	260	460	700	1000	1200	1300	1500
Each side nozzle									
F_x	160	240	320	560	850	1200	1500	1600	1900
F_y	130	200	260	460	700	1000	1200	1300	1500
F_z	200	300	400	700	1100	1500	1800	2000	2300
Each end nozzle									
F_x	200	300	400	700	1100	1500	1800	2000	2300
F_y	130	200	260	460	700	1000	1200	1300	1500
F_z	160	240	320	560	850	1200	1500	1600	1900
Each nozzle									
M_x	340	700	980	1700	2600	3700	4500	4700	5400
M_y	260	530	740	1300	1900	2800	3400	3500	4000
M_z	170	350	500	870	1300	1800	2200	2300	2700

NOTE: F = force, in pounds; M = moment, in foot-pounds; Subscript x = horizontal (parallel to horizontal shafts); Subscript y = vertical (parallel to vertical shafts); Subscript z = horizontal (parallel to side nozzle centerlines). See Figure 1 for a diagram of the coordinate system. For vertical and in-line pumps that are turbine driven, use values for side nozzles; for vertical and in-line pumps that are motor driven, multiply values for side nozzles by 2.

[a] In summing moments about any point, the forces, F, multiplied by their respective moment arms are to be added to the moments, M, to give the total moment.

[b] These values are for guidance only and are subject to negotiation between the purchaser and the vendor for the specific application.

Figure 6. Nozzle Loadings and Associated Coordinate System (Extracted from API-610 Sixth Edition).

tions which can be used to predict pump casing design modifications which will limit the shaft displacement at the coupling to 0.002 inch.

ASSUMPTIONS

1. The body of the casing is rigid relative to the attachment feet.

2. The pump casing material has a modulus of rigidity equal to 11.5×10^6 PSI (Cast Steel).

3. All loads other than those moments about the Z axis cause negligible shaft displacement and can be ignored.

4. The maximum resultant Z moment, $(MZC)_{MAX}$, due to Table 2 Piping Loads, produces a deflection at the pump shaft coupling hub equal to 0.002 inch.

$$J_{MIN} = \frac{(5.2 \times 10^{-4}) \times (MZC)_{MAX} \times L_2 \times W}{\left(\frac{L_2}{L_1} + 1\right)} \quad (1)$$

$$MZC = MZS + MZD - [(FXS)(YS) + (FXD)(YD) - (FYS)(XS) - (FYD)(XD)]/12 \quad (2)$$

$$J_{ACT} = B_f L_f T_f^3 + B_r T_r^3 \quad (3)$$

In establishing the value of J_{MIN}, it is necessary also to establish $(MZC)_{MAX}$. This value is obtained from Equation (2) using API-610 Table 2 Loads (Figure 6) with appropriate signs to max-

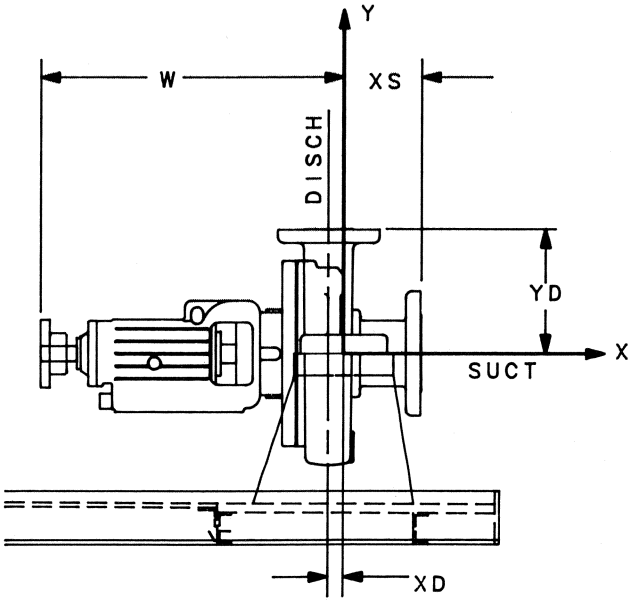

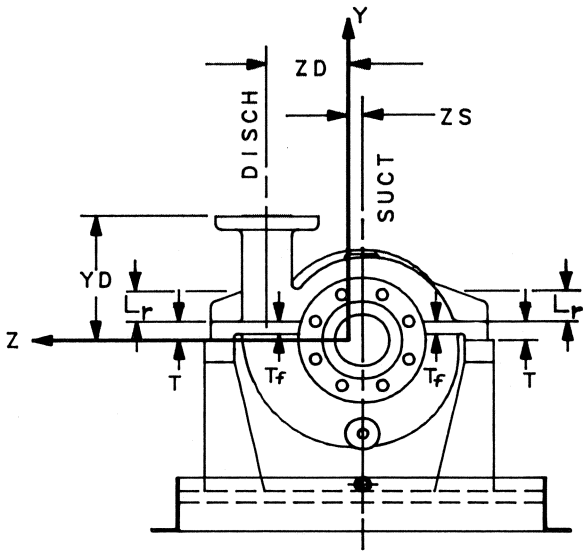

Figure 7a. End Suction Overhung Process Pump Nomenclature.

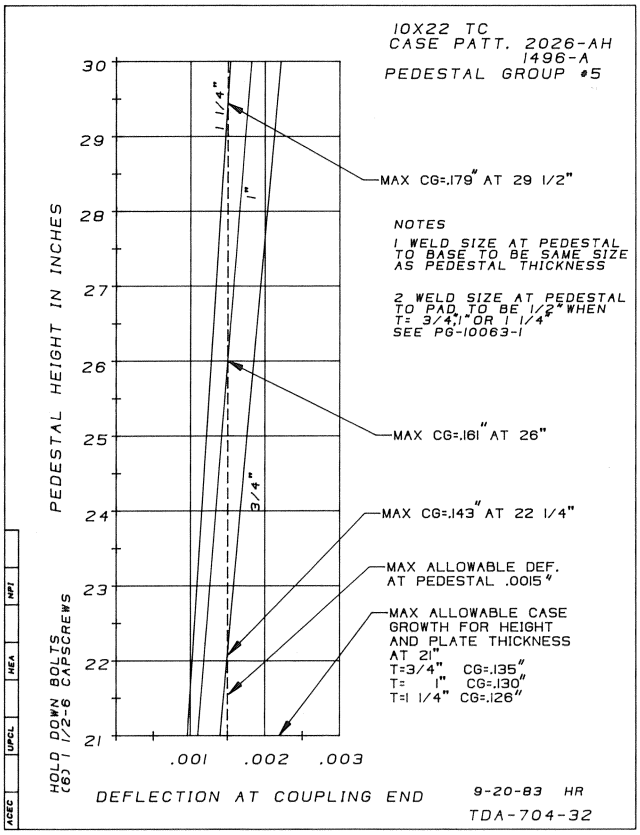

Figure 12. Computer Generated Pedestal Selection Chart.

.0015 inch subcomponent stiffness criteria.

If casing thermal growth, as illustrated in Figure 11, is not absorbed in an acceptable manner, pump operability may be affected due to shaft misalignment [2]. Shaft misalignment can be caused by: 1) unsymmetrical support pedestals that twist or do not absorb casing thermal growth equally, 2) sliding of the pump across the support pedestal pads as a result of insufficient hold-down capscrew preload, 3) permanent distortion (yielding) of the load carrying members due to insufficient support pedestal flexibility.

Our computer generated pedestal selection charts (Figure 12) are used to ensure that support pedestals are stiff enough to meet the .0015 inch deflection criteria, yet flexible enough to absorb the casing thermal growth without causing undue shaft misalignment. The solid lines identified in Figure 12 as (¾, 1, 1¼) represent pedestal plate thickness while CG is the allowable casing thermal growth which must be greater than the calculated thermal growth established by Figure 13 and Equation (9). To meet the subcomponent stiffness criteria, the deflection at the coupling end must be less than the allowable value which is nominally 0.0015 inch and is indicated by the dashed vertical line.

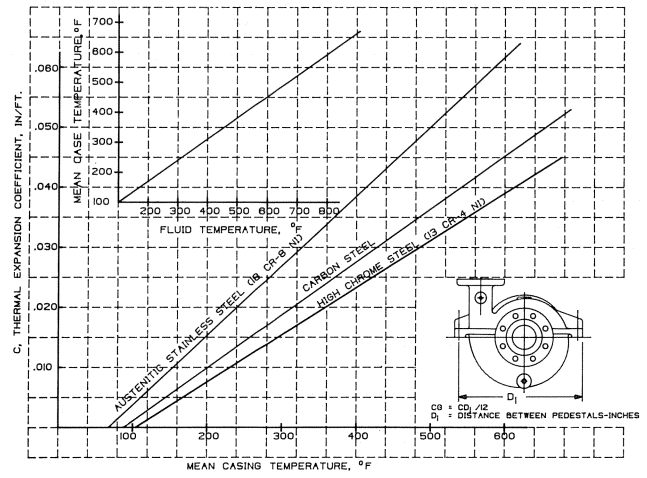

Figure 13. Horizontal Process Pump Thermal Expansion Chart.

EXPERIMENTAL TESTING

Experimental testing has been conducted to verify that the analytical procedures previously described produce equipment that meets API's design criteria. Loads up to two times $(MXC)_{MAX}$, $(MYC)_{MAX}$, $(MZC)_{MAX}$ were applied to assembled pumps by hanging known weights to piping attached to the suction and discharge nozzles (Figure 14). For each load increment, an operability test (paragraph 2.4.2) and a stiffness test (paragraph 2.4.3) were performed. By neglecting the effect of internal pressure (radial hydraulic load), a simple test for operability was devised: To detect any internal contact of rotating and stationary components due to the imposed piping loads, the rotor was rotated by hand. To date, no perceptible rubbing has been felt. Assembly stiffness was measured in terms of shaft displacement at the coupling. A digital voltmeter and three noncontacting eddy current probes were used to measure shaft movement in the X, Y, Z directions (Figure 15).

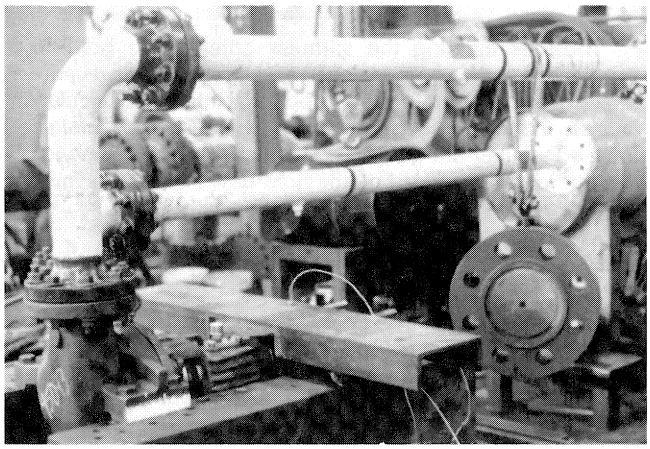

Figure 14. Side View of an Overhung Process Pump Case Stiffness Test Set-Up.

Factory tests were conducted with assembled pumps bolted to large rigid shop pedestals secured to a bedplate. The proximity probes were attached to a 9-inch channel which was supported by the shop pedestals. With this test arrangement, the effect of support pedestal flexibility has been eliminated. This means that the measured shaft deflection at the coupling will be due to flexibilities in the pump casing (0.002 inch) and the hold-down capscrews (0.0015 inch). Test results for three overhung process pumps are presented graphically in Figures 16-18. All graphs are plotted to the same scale to illustrate that the pump casing is most sensitive to moments about the Z axis. To demonstrate "trends" as a function of pump size and load orientation, displacements acting in the same direction have been connected by solid, dashed and dotted lines in these figures. This experimental data indicates that the attachment foot and hold-down capscrew sizing procedures are satisfactory for predicting design modifications. The data also indicated that

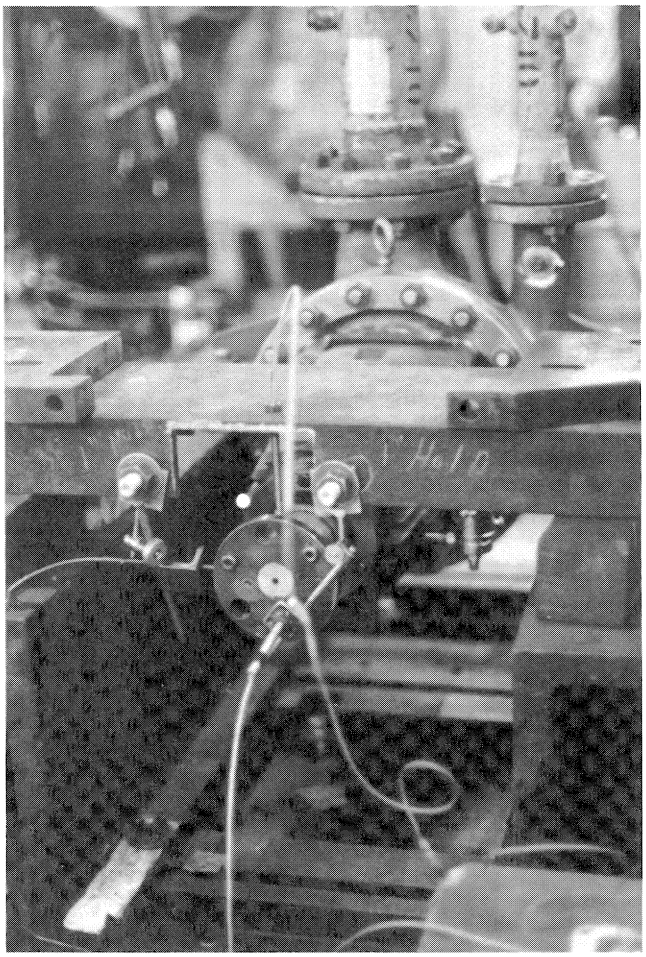

Figure 15. End View of an Overhung Process Pump Case Stiffness Test Set-Up.

the Z displacement due to moments about the Y axis may not be negligible and that these pump casings would be unacceptable for a heavy-duty baseplate application.

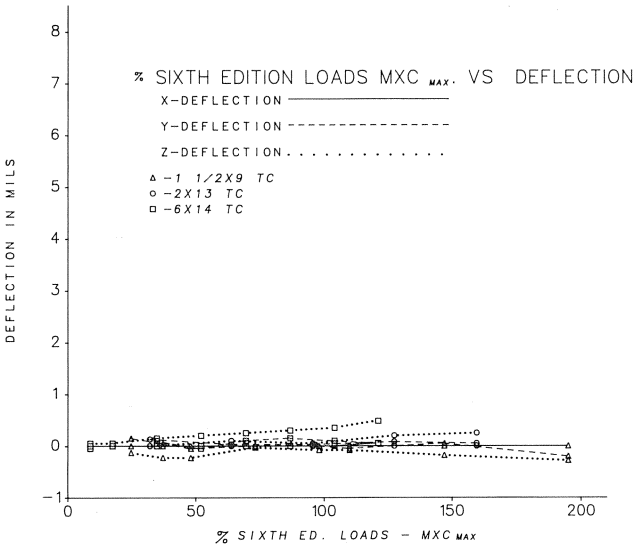

Figure 16. Experimental Pump Case and Hold-Down Capscrew Stiffness Data for MXC Moments.

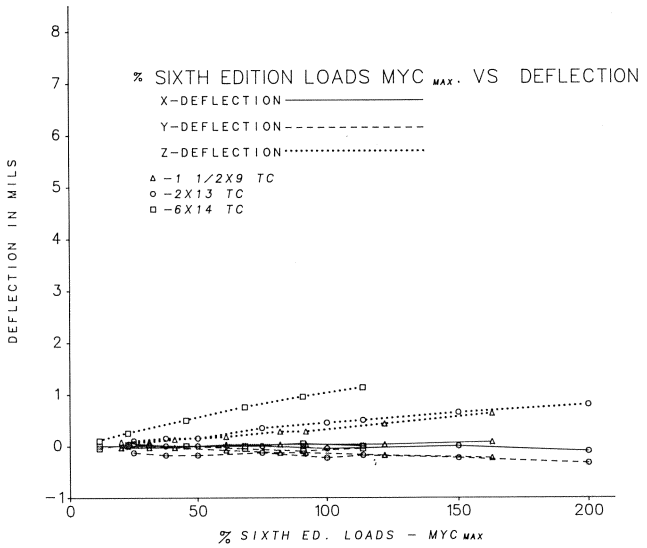

Figure 17. Experimental Pump Case and Hold-Down Capscrew Stiffness Data for MYC Moments.

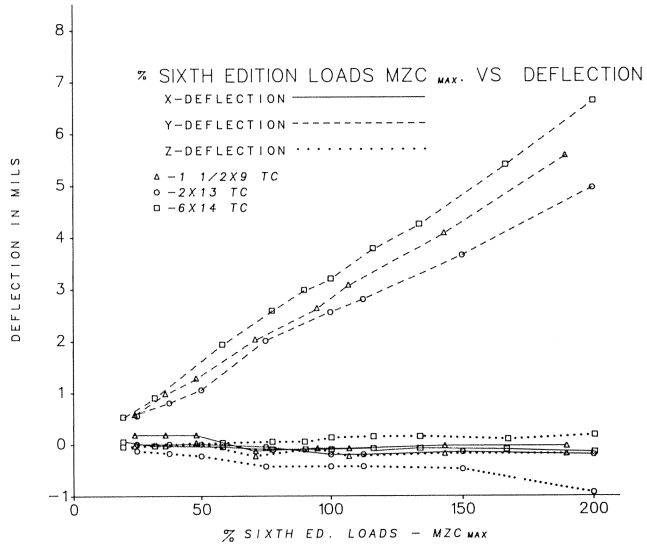

Figure 18. Experimental Pump Case and Hold-Down Capscrew Stiffness Data for MZC Moments.

The results of field tests conducted on a 3 × 9 TC pump mounted on its 6th Edition baseplate are illustrated in Figure 19. The test set-up was similar to that previously described, except shaft displacements at the coupling hub were measured relative to the concrete foundation. This was done to take into account support pedestal and baseplate flexibilities. The magnitude of the applied moments was also limited by the available working space. The field data shown in Figure 19 are remarkably similar to the case stiffness test data illustrated in Figures 16, 17 and 18. The calculated overall displacement at the coupling hub assuming that $(MXC)_{MAX}$, $(MYC)_{MAX}$, $(MZC)_{MAX}$ moments occur simultaneously is 3.63 mils. This verifies that the 3 × 9 TC pump, when mounted on its grouted-in baseplate, meets API-610 nozzle loading requirements.

HEAVY-DUTY BASEPLATES

Paragraph 2.4.6 states that an optional heavy-duty baseplate can be supplied which will double the stiffness of the pump, baseplate, and support pedestal assembly. Calculations

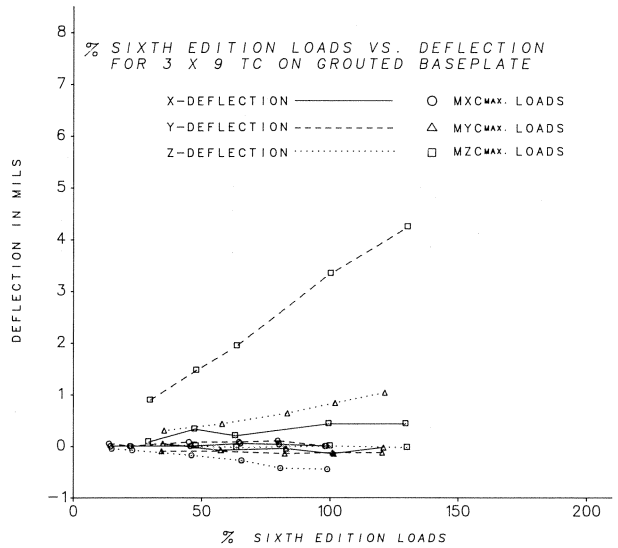

Figure 19. Experimental Pump and Baseplate Stiffness Data.

and test data indicate that a heavy-duty baseplate alone cannot meet this requirement. Assuming that a perfectly rigid baseplate and pedestal support structure (cold product applications) could be designed and manufactured, the pump casing and hold-down capscrew deflection criteria would need to be changed from 0.0035 inch to 0.0025 inch based on Table 2 piping loads. Special thick-walled pump casings would probably be required since the standard 6th Edition attachment feet are stiffer than the pump casing.

According to API-610, the purpose of the heavy-duty baseplate was to simplify piping layouts by allowing higher loads from the attached piping. In most instances high piping loads occur when hot product is being handled. In these applications, the support pedestals must have flexibility in order to absorb pump casing thermal expansion. For this reason, we do not feel that it is advisable to furnish stiffer support pedestals. Assuming that the support pedestal stiffness is not increased, the deflection criteria for the pump casing and hold-down capscrews must be changed from 0.0035 inch to 0.001 inch using Table 2 loads as a basis. This means that special thick-walled pump casings would need to be about 3½ times stiffer than the standard 6th Edition casings previously described. Obviously, this is not a practical solution to the heavy-duty baseplate requirement.

We believe that contractors and users would be better off to specify standard 6th Edition baseplates and submit component piping loads when they exceed Table 2 (Figure 6) values. In most instances higher component piping loads can be imposed and still meet the 0.005 inch deflection criteria. This is particularly true when MZC_{MAX} based on actual piping loads is less than MZC_{MAX} based on API-610 Table 2 loads. If the component piping loads are too large to meet the 0.005 inch deflection criteria, we can supply the contractor with pump nozzle and pedestal support stiffnesses which can be input into the piping flexibility analysis. Pumps are normally modelled as rigid pipe anchors; introducing nozzle and pedestal flexibilities into the computer model generally results in smaller component piping loads.

NOMENCLATURE

A_{MIN}	Required hold-down capscrew tensile stress area (in^2) to limit shaft displacement at the coupling to 0.0015 inch and to prevent sliding at the pump foot pad to support pedestal interface.
B_f, B_r	Torsional coefficient from Figure 9 for pump feet or ribs.
d	Nominal diameter (in) of the pump hold-down capscrews.
D_c	Hold-down capscrew displacement (in) that will produce a 0.0015 in deflection at the pump shaft coupling hub due to rigid body rotation of the pump casing.
D_0,D_1,D_3	Dimensions (in) used to define the hold-down capscrew pattern (Figure 10).
FXC,FYC,FZC	Resultant forces (lbs) acting at the center of the pump in the X, Y or Z direction due to suction and discharge nozzle component forces.
FXD,FYD,FZD	Component forces (lbs), extracted from Table 2 of API-610, 6th Edition, acting on the discharge nozzle flange facing in the X, Y or Z direction.
FXP,FZP	X or Z component of the resultant horizontal shear force (lbs) per hold-down capscrew due to Table 2 piping loads.
FXS,FYS,FZS	Component forces (lbs), extracted from Table 2 or API-610, 6th Edition, acting on the suction Nozzle flange facing in the X, Y or Z direction.
$(FY)_{MAX}$	Maximum axial force (lbs) per hold-down capscrew due to API-610 Table 2 nozzle loads.
FZT	Horizontal shear force (lbs) per support pedestal due to casing thermal expansion. Evaluated with computer program baseload.
J_{ACT}	Actual torsional constant (in^4) of a pump foot.
J_{MIN}	Minimum acceptable torsional constant (in^4) for a pump foot which will limit shaft deflection at the coupling hub to 0.002 inches for a given $(MZC)_{MAX}$ moment.
L_f	Effective length (in) of a pump foot parallel to the pump shaft (Figure 8).
L_r	Effective length of a pump foot rib (Figure 7).
L_1	Effective length (in) of a pump foot opposite the discharge nozzle and perpendicular to the pump shaft (Figure 8).
L_2	Effective length (in) of the pump foot on the discharge nozzle of the casing and perpendicular to the pump shaft (Figure 8).
MXC,MYC,MZC	Resultant moment (ft/lbs) about the X, Y or Z axis based on component piping loads (Table 2 of API-610) resolved to a coordinate system located at the center of the pump.
MXD,MYD,MZD	Components moments (ft/lbs), extracted from Table 2 of API-610, acting on the discharge nozzle flange facing about the X, Y and Z axis.
MXS,MYS,MZS	Component moments (ft/lbs), extracted from Table 2 of API-610, acting on the suction nozzle flange facing about the X, Y or Z axis.
N	Total number of hold-down capscrews.

PL	Hold-down capscrews proof load (psi).
T	Thickness (in) of the pump foot in the vicinity of the hold-down capscrews (Figure 7).
T_f	Thickness (in) of the pump foot at the foot to casing junction (Figure 7).
T_r	Thickness (in) of the pump foot ribs (Figure 8).
W	Distance (in) from the center of the pump foot to the face of the pump shaft coupling hub (Figure 7).
XD,YD,ZD	Location coordinates (in) of the discharge nozzle flange facing (Figures 7 and 8).
XS, YS, ZS	Location coordinates (in) of the suction nozzle flange facing (Figures 7 and 8).

REFERENCES

1. American Petroleum Institute, "Centrifugal Pumps for General Refinery Services," *API Standard 610, Sixth Edition,* pp. 6-7 (1981).
2. Simon, C. A., "Allowable Pump Piping Loads," Hydrocarbon Processing pp. 98-101 (June 1972).
3. Bussemaker, E. J., "Design Aspects of Baseplates for Oil and Petrochemical Industry Pumps," Mechanical Engineering C 45-81, pp. 135-141 (1981).

ACKNOWLEDGEMENTS

The author thanks United Centrifugal Pumps for permission to publish this article and Standard Oil Company of California for their cooperation in field testing.